Journal of Bioscience and Bioengineering
VOL. 128 No. 5, 613–621, 2019

www.elsevier.com/locate/jbiosc

Characterization of silver nanoparticle-modified decellularized rat esophagus for esophageal tissue engineering: Structural properties and biocompatibility

Tarek Saleh,[1,‡] Ebtehal Ahmed,[1,‡] Lina Yu,[1] Ho-Hyun Kwak,[1] Byung-Jae Kang,[1] Kyung-Mee Park,[2] Ki-Young Choi,[3] Byeong-Moo Kim,[4] Kyung-Sun Kang,[5] and Heung-Myong Woo[1,*]

Department of Veterinary Science, College of Veterinary Medicine and Institute of Veterinary Science, Kangwon National University, Chuncheon 200-701, Republic of Korea,[1] College of Veterinary Medicine, Chungbuk National University, Cheongju, Chungbuk 28644, Republic of Korea,[2] Department of Controlled Agriculture, Kangwon National University, Chuncheon, Gangwon 200-701, Republic of Korea,[3] Department of Medicine, GI Unit, Massachusetts General Hospital and Harvard Medical School, Boston, MA 02114, USA,[4] and Research Institute for Veterinary Science, College of Veterinary Medicine, Seoul National University, Seoul 08826, Republic of Korea[5]

Received 2 December 2018; accepted 17 April 2019
Available online 22 May 2019

Decellularized esophageal matrices are ideal scaffolds for esophageal tissue engineering. Unfortunately, in order to improve transplantation possibilities, they require modification to reduce their degradation rate and immunogenicity. To date, no modifying agent has been approved to overcome these limitations. The objective of this study was to evaluate the ability of silver nanoparticles (AgNPs) to improve the structural stability and biocompatibility of decellularized rat esophagi. AgNPs have the advantage over currently used agents in that they bind with collagen fibers in a highly ordered manner, via non-covalent binding mechanisms forming multiple binding sites, while other agents provide only two-point connections between collagen molecules. Rat esophagi were decellularized, loaded with 5 μg/mL of AgNPs (100 nm), and then treated with an immobilization-complex buffer composed of ethyl carbodiimide hydrochloride and N-hydroxysuccinimide (EDC/NHS). Then, they were evaluated in terms of ultra-structural morphology, water uptake, *in vitro* resistance to enzymatic and thermal degradation, indentation strength, *in vitro* anti-calcification, cyto-compatibility with rat bone marrow derived stromal cells (rat-BMSCs), angiogenic properties, and *in vivo* biocompatibility, and compared to scaffolds modified using glutaraldehyde and EDC/NHS complex buffer alone. AgNP-modified scaffolds showed an improved ultrastructure, good water uptake, and considerable resistance against *in vitro* degradation and indentation, and a high resistance against *in vitro* calcification. Moreover, they were cytocompatible for allogeneic rat-BMSCs. Additionally, AgNPs did not alter the angiogenic properties of the modified scaffolds and decreased host immune responses after their subcutaneous implantation. The structural properties and biocompatibility of decellularized esophageal matrices could be improved by conjugation with AgNPs.

[**Key words:** Esophagus; Tissue engineering; Decellularization; Cross-linking; Biocompatibility; Silver nanoparticles]

Esophageal disorders, including congenital defects, traumatic injuries and cancers, are complicated by lack of regeneration and scarification, and so are associated with high mortalities. Tissue-engineered gastrointestinal tract scaffolds are promising means for reconstructing a variety of esophageal defects. However, selecting appropriate scaffolds remains challenging as such scaffolds should provide a functional native-mimic tissue, and lack the tendency to degrade quickly or to calcify after grafting, in order to be suitable for esophageal tissue reconstruction (1–3). Despite decellularized full-thickness esophagus being recognized as the most suitable scaffold for regeneration of injured esophagus, it has the similar limitations to those found in other collagenous tissues, including rapid biodegradation and immunogenicity (4–6).

Glutaraldehyde is the oldest and most common crosslinking agent used to overcome the above-mentioned limitations, but unfortunately, it may detrimental alter the turnover process of the scaffolds' collagenous materials. Although the disadvantages of glutaraldehyde may be avoided using genipin, a natural cross-linking agent, its complex extraction process, high cost, and the blue coloration induced in treated tissues are major limitations for genipin's wider application (7,8).

Recently, researchers attempted to modify various decellularized scaffolds with different nanomaterials to improve the structural and functional properties of their various decellularized scaffolds (9–12). One of the most interesting nanoparticles used in various fields are silver nanoparticles (AgNPs); recently, they have attracted increasing attention. AgNPs have a broad range of biomedical applications mainly owing to their anti-bacterial and anti-inflammatory activities (13–18). Moreover, they have unique properties which allow for multiple site attachments; they bind with collagenous material in a highly ordered manner through electrostatic and/or hydrophobic interactions (14,19). Our team has succeeded in conjugating AgNPs with decellularized porcine livers in an attempt to overcome the limitations of previous crosslinking

* Corresponding author at: Department of Veterinary Surgical Sciences, College of Veterinary Medicine, and Stem Cell Institute, Kangwon National University, Hyojadong 192-1, Chuncheon, Gangwon 200-701, Republic of Korea. Tel.: +82 33 250 8651 8981; fax: +82 33 244 2367.
E-mail address: woohm@kangwon.ac.kr (H.-M. Woo).
‡ These authors contributed equally to this work.

1389-1723/$ – see front matter
https://doi.org/10.1016/j.jbiosc.2019.04.017

methods (18). The aim of this study was to evaluate the ability of AgNPs (100 nm) to improve the structural stability and biocompatibility of decellularized rat esophagus.

MATERIALS AND METHODS

Harvesting and decellularization of rat esophagi Esophagi were harvested from 8-week-old male Sprague–Dawley rats, and the lumens perfused with 1x PBS for 30 min (5 ml/min), which was followed by perfusion with a 0.1% solution of sodium dodecyl sulfate (SDS) for 6 h (5 ml/min). Then, they were washed with PBS for 2 h (5 ml/min).

Gross and microscopic examinations, and scanning electron microscope imaging The transparency of the decellularized esophagi was evaluated by gross examination with the naked eye. Histological examination was performed using hematoxylin and eosin (H&E) staining on paraffinized sections from decellularized esophagi to evaluate cellular removal and to examine the structural integrity of the decellularized scaffolds in comparison with the native ones. Additionally, 4,6-diamidino-2-phenylindole (DAPI) staining was performed to confirm the complete removal of cells. Imaging under a scanning electron microscope (SEM) (KBSI, Chuncheon Center, Seoul, South Korea) was also performed to confirm the complete removal of cells and the preservation of the extracellular matrix (ECM) ultrastructure.

Quantification of DNA Total DNA was extracted using a G-spin Total DNA Extraction Kit (iNtRON Biotechnology, Seoul, Korea) according the manufacturer's instructions. The genomic DNA content was then evaluated via agarose gel electrophoresis, using a 100 bp DNA ladder, and a Nanodrop spectrophotometer ND-1000 (PeqLab, Erlangen, Germany).

Biochemical analyses Collagen and sulfated glycosaminoglycans (sGAG) were measured using Sircol and Blyscan assay kits (Biocolor Ltd, Carrickfergus, UK), respectively, according to the manufacturer's instructions.

Immunofluorescent staining To confirm the presence of different ECM proteins in decellularized tissues such as collagen I, fibronectin, and laminin, polyclonal rabbit anti-collagen I (ab34710, Abcam, Cambridge, UK), polyclonal rabbit anti-fibronectin (ab2413, Abcam), and polyclonal rabbit anti-laminin (ab11575, Abcam) antibodies were used as primary antibodies. Goat anti-rabbit IgG (Alexa flour 647, ab150079, Abcam) was used as the secondary antibody. Their expressions were visualized using a fluorescence microscope (Olympus, Tokyo, Japan).

Modification of decellularized esophageal scaffolds Decellularized esophagi were cut into circular segments with a length of 3 mm, and then immersed with shaking for 4 h at 37°C in different solutions of: (i) 100 nm AgNPs (730777, Sigma–Aldrich, St. Louis, MO, USA) (5 μg/mL) (AgNP group); (ii) 0.625% glutaraldehyde (Glut group); (iii) 0.6% ethyl carbodiimide hydrochloride (EDC)/ 0.36% *N*-hydroxysuccinimide (NHS) complex in 1.06% 2-(*N*-morpholino) ethanesulfonic acid (MES) buffer (EDC/NHS group); and (iv) ultra-pure water as a control (decellularized unmodified or DL group). Next, the esophageal segments from the AgNP group were rinsed in PBS and immersed in an immobilization buffer consisting of the EDC/NHS complex in MES buffer for 30 min to immobilize the loaded nanoparticles. Then, the segments from all groups were rinsed in PBS for 48 h.

Ultrastructural analysis SEM imaging was performed to evaluate the structural improvements in the different modified scaffolds, in comparison with the unmodified decellularized scaffolds.

Swelling ratio A swelling test was performed according to the procedure of Yan et al. (20). Air-dried segments from different groups (n = 3 for each) were weighed (W0) and then immersed for 3 h in PBS at room temperature. After removal of excess water, the wet segments were weighed (W1) again, and their swelling ratio calculated as the wet weight increase to the initial dry weight (W1- W0/W0).

***In vitro* collagenase resistance** The resistance of esophageal segments from the different experimental groups to collagenase digestion was evaluated by ninhydrin assay and Sircol Collagen Assay. Briefly, dry esophageal segments (n = 6 for each group) were immersed in 0.1 M Tris–HCl containing 50 mM calcium chloride and incubated at 37°C for 30 min. They were then treated with 0.1 M Tris–HCl containing 50 units of collagenase type I (Worthington Biochemical Co., Lakewood, NJ, USA) and incubated with shaking at 37°C for 12 h. The samples were treated with 0.25 M of ethylenediaminetetraacetic acid (EDTA, MediaTech Inc., Manassas, VA, USA) on ice to stop digestion. The amino acids released after *in vitro* biodegradation from the segments representing the different groups were visualized by ninhydrin reaction. Briefly, lysates of degraded segments from the different groups were centrifuged, after which the supernatants were hydrolyzed (6 N HCl, 110°C). Ninhydrin solution (Sigma Aldrich, St. Louis, MO, USA) was then added and the mixtures were heated for 30 min at 100°C. The optical densities (ODs) of the mixtures from the different groups were measured using a UV-vis spectrophotometer at a wavelength of 570 nm and evaluated semi-quantitatively by dividing the values of the ODs of the mixtures from the different treated groups by those from the DL group. Additionally, to detect the amount of the collagen remaining in the segments after *in vitro* biodegradation, the insoluble collagen content was estimated using a Sircol collagen assay kit (Biocolor, Carrickfergus, UK), according to the manufacturer's instructions and evaluated by dividing the values of the different treated groups by those from the DL group.

Thermal degradation The denaturation temperature was estimated using a differential scanning calorimeter (Q2000 DSC, TA Instruments, New Castle, DE, USA) to evaluate the improvements in the physicochemical properties or thermal stabilities of the decellularized esophagi from the different crosslinking groups (4,21). Samples from the different groups (n = 3 for each group) were heated from 0°C to 110°C at a rate of 5°C per minute in a nitrogen atmosphere. The point of denaturation was determined using the heat flow/temperature curve.

Indentation strengths The indentation test for the scaffolds from the different groups was performed using the CT3 Texture analyzer (Brookfield Engineering Laboratories, Middleboro, MA, USA) (22–24). Then, the indentation strengths were evaluated by dividing the values of the different treated groups by those from the DL group.

***In vitro* anti-calcification properties** Alizarin Red S (ARS) staining assay was used to evaluate the *in vitro* anti-calcification properties of the scaffolds from the different groups after their incubation in simulated body fluid, which has ion concentrations similar to those of the normal blood plasma (25–27). Equally weighted samples (n = 3 for each group) were incubated in simulated body fluid with agitation for 7 days at 37°C. The samples were then washed with deionized water, immersed in Alizarin Red S for 30 min, and washed again with deionized water. Next, they were immersed in 50% acetic acid to extract the bound stain. The final pH of the different solubilized stains (pH = 4.1) was adjusted using sodium hydroxide (1 M). Lastly, their absorbances at 550 nm were measured using a UV spectrophotometer.

***In vitro* cytocompatibility** Extraction-MTT assay was performed to test the cytocompatibility of scaffolds from the different groups using rat bone marrow mesenchymal stem cells (rat BM-MSCs). Conditioned medium from the different groups was obtained by incubating the scaffolds in DMEM (0.2 mg/ml) for 3 days at 37°C. The effects of the different conditioned media on the viability of pre-cultured bone marrow rat mesenchymal stem cells (passage No. 3), isolated according to the method of Zhang and Chan (28), were evaluated quantitatively using an extraction-MTT assay (Sigma Aldrich) after adding 10% FBS and 1% penicillin. Normal media and dimethyl sulfoxide (DMSO) were used as negative and positive controls, respectively. OD values of MTT formazan at 570 nm of the DL and different modified groups were divided by that of the negative control group to calculate the percentage of cell viability.

Angiogenic properties Scratch-induced directional wounding migration assay was performed to test whether the modification of the decellularized esophageal scaffold in the different groups alters their angiogenic properties (29). EA.hy 926 endothelial cells were cultivated in 12-well gelatin-precoated plates in DMEM until the confluence of cells reached 90%. Next, scratches (one scratch per well) were made using a cell scraper, after which the cells were imaged, and their widths were calculated (T0). Then, the wells were washed thrice with PBS, followed by the addition of the conditioned media from the different groups (that were prepared as mentioned previously for the extraction-MTT assay). Finally, the scratched defects were imaged, and their widths were calculated (TA) after 2 days to estimate the wound confluence %. Normal DMEM was used as a control.

***In vivo* biocompatibility** All procedures were performed in accordance with the ethical and scientific guidelines of the Institutional Animal Care and Use Committee (IACUC) of Kangwon National University, South Korea. Native, non-modified decellularized, and the various modified decellularized esophageal segments were sterilized by immersing and shaking in 0.1% peracetic acid (PAA; Sigma Aldrich) for 2 h, followed by washing with PBS for 48 h. Thirty ICR male mice (4 weeks old) were anesthetized, a small incision made down the back of the animals, and then a dorsal subcutaneous pouch was created by blunt dissection. An esophageal segment was implanted into this pouch, oriented away from the suture site, and the wound was sutured. Animals were euthanized at 7 and 21 days post-implantation (PI).

Different groups were evaluated by H&E staining to qualitatively evaluate local inflammatory responses against their segments, and quantitatively by counting neutrophils and lymphocytes within five histological fields (400 x) per animal of the different groups at 7 and 21 days PI. Additionally, immunofluorescent (IF) staining was performed in order to detect macrophage phenotypes (M1: proinflammatory and M2: anti-inflammatory) at 7 and 21 days PI using an anti-CD68 antibody (Alexa Fluor 405, cat. no. ab199571, Abcam) as a pan-macrophage (MΦ) marker, an anti-CCR7 antibody (Alexa Fluor 555, cat. no. ab207018, Abcam) as an M1 marker, and an anti-CD206 antibody (Alexa Fluor 594, cat. no. 141726, BioLegend, San Diego, CA, USA) as an M2 marker. M1/M2 ratios were calculated using Image J software.

Evaluation silver nanoparticle retention on esophageal scaffolds Esophageal segments from the AgNP group (n = 3) were immersed in sterile ultrapure water (5 mL) and incubated at 37°C for 7 days with agitation. After centrifugation, the UV-vis absorption of 2 mL of the supernatant was measured

in a range of 350–850 nm twice per day (every 12 h). The withdrawn volume was replaced with an equal amount of fresh ultrapure water after each measurement. Esophageal segments from the EDC/NHS group and ultrapure water were used as the blank and control samples, respectively.

Statistical analyses DNA quantities and results from the biochemical analyses of native and decellularized esophagi were analyzed statistically using the Student's *t*-test, while univariate analysis of variance (ANOVA) with Tukey's honestly significant difference (HSD) post hoc multiple comparison test was performed to evaluate differences between the different modified groups. All tests were performed using statistical software (IBM SPSS version 21).

RESULTS

Characterization of decellularized esophageal scaffolds As shown in Fig. 1A–H, decellularized esophagi displayed white translucent coloration. The complete removal of cells and maintenance of the native structure was observed with H&E staining, and confirmed with DAPI staining, which showed absence of nuclear content in decellularized esophagi. Moreover, SEM imaging confirmed the well-preserved condition of the ECM structure in decellularized esophagi, which was comparable to that of native esophagi. No DNA fragments (markers of cell remnants) were detected in the decellularized tissues via DNA gel electrophoreses (Fig. 1I). In addition, DNA quantification showed that DNA content within the decellularized esophagi was decreased significantly (P =0.0004) (Fig. 1J). Following biochemical analyses, there was no significant difference (P = 0.0757) between the collagen contents of the native and decellularized esophagi (Fig. 1K). The sGAG content decreased significantly (P = 0.0377) in decellularized esophagi compared with that in native slices (Fig. 1L). In addition, IF staining confirmed retention of different ECM proteins in decellularized tissue scaffolds (Fig. 1M).

Evaluation of the modifying effects of different agents on the decellularized esophagi Evaluation with SEM imaging showed that the ultrastructure of the submucosal layer of the different modified esophagi revealed structural improvements in comparison to the decellularized esophagi. Compared to the samples from the Glut group, in which the pore spaces between the collagen fibers were markedly decreased, the samples from the AgNP group showed the binding of collagen fibers without extensive alterations of the pore areas. Moreover, samples from the AgNP group displayed a more regular binding of collagen fibers compared to the case for the EDC/NHS group. Additionally, the nanoparticles did not aggregate with each other to a large extent (Fig. 2A).

With regards to water uptake, the swelling ratios of the different modified groups were significantly lower ($P < 0.05$) than that of the DL group; however, the AgNP group showed a significantly higher swelling ratio compared to both the Glut and EDC/NHS groups ($P < 0.05$) (Fig. 2B).

With regards to the *in vitro* resistance of the different modified scaffolds to collagenase, as determined by means of the ninhydrin assay, the mean ratio of ODs of samples from the AgNP group was significantly higher than that in case of the Glut group ($P < 0.05$). The EDC/NHS group showed the highest percentage of mean ratio of ODs when compared to the case for the other modified groups ($P < 0.05$) (Fig. 2C). Moreover, the ratio of the remaining collagen content of the Glut group was significantly higher than that of the AgNP group ($P < 0.05$). The ratio of samples from the EDC/NHS group was the lowest among all the modified groups ($P < 0.05$) (Fig. 2D).

With regards to the thermal degradation and indentation results, the samples in the Glut group showed the highest mean values among all groups ($P < 0.05$), while those in the AgNP group showed the second highest values, with significant differences compared to the DL and EDC/NHS groups ($P < 0.05$) (Fig. 2E,F).

With regards to the anti-calcification properties, as shown in Fig. 2G, among all groups, the samples from the AgNP group showed the lowest mean value of the absorbances of the Alizarin Red S staining ($P < 0.05$). The samples from the Glut group showed a significantly higher mean value of the absorbances ($P < 0.05$) than that of samples from the DL group, which showed no significant difference ($P \geq 0.05$) compared with the values of samples from the EDC/NHS group.

Evaluation of *in vitro* cytocompatibility using rat BM-MSCs In the extraction-MTT assay, no significant differences ($P \geq 0.05$) in the viability of rat BM-MSCs were detected between the different groups, with the exception of the Glut group, which showed a significant decrease ($P < 0.05$) in the cell viability (Fig. 2H).

Evaluation of the angiogenic properties for each type of modification As shown in Fig. 3, compared to the DL group, in both the EDC/NHS and AgNP group, no deleterious effects on the scratch-induced migration of the endothelial cells ($P \geq 0.05$) were observed, while in the Glut group, significant alterations of the migration and proliferation of the endothelial cells ($P < 0.05$) were observed.

Evaluation of the *in vivo* biocompatibility of the different modified scaffolds As shown in Fig. 4A under H&E staining, the native group exhibited an intense host immune response, while the other groups showed only mild host responses at 7 and 21 days PI. The scaffolds from the AgNP group showed the lowest number of infiltrated inflammatory cells at both 7 and 21 days PI, with significant differences ($P < 0.05$) only at 7 days PI. Other modified groups were not significantly different when compared to one another ($P \geq 0.05$) (Fig. 4B).

From IF staining of macrophages (M1 and M2) at days 7 and 21 PI, the native group showed significantly higher mean M1/M2 ratios at both times of examination when compared with other groups ($P < 0.05$). Among the unmodified and modified decellularized scaffold groups, significantly higher mean M1/M2 ratios were observed in the Glut group ($P < 0.05$), whereas the AgNP group showed the lowest ratios, but with no significant differences compared to the ratios from the DL and EDC/NHS groups at both 7 and 21 days after implantation ($P \geq 0.05$) (Fig. 5).

Evaluation of silver nanoparticles retention on esophageal scaffolds No characteristic AgNP peak was detected by means of UV-vis spectrophotometry over the course of one week in the collected ultrapure water supernatants used to immerse the esophageal segments from the AgNP group (data not shown).

DISCUSSION

Reducing the limitations associated with decellularized esophageal scaffolds is important for increasing their clinical usefulness in transplantation. Our hypothesis in this study is that loading decellularized rat esophageal scaffolds with AgNPs may improve their structural stability and biocompatibility, principally because the ability of AgNPs to bind to collagen fibers, in combination with their anti-inflammatory effects, improves collagen fiber stability, and reduces host immune responses against decellularized natural tissue-derived scaffolds. To the best of our knowledge, this is the first study to use nanoparticles to modify the structural and biocompatibility properties of decellularized esophageal scaffolds.

Chemical composition of the AgNPs In the current study, we used citrate-stabilized AgNPs without amine functionalization. This is because the functionalization process may cause the nanoparticles to aggregate, which alters their homogeneous distribution within the scaffolds (30). The binding mechanism of citrate-stabilized AgNPs depends on their ability to physically

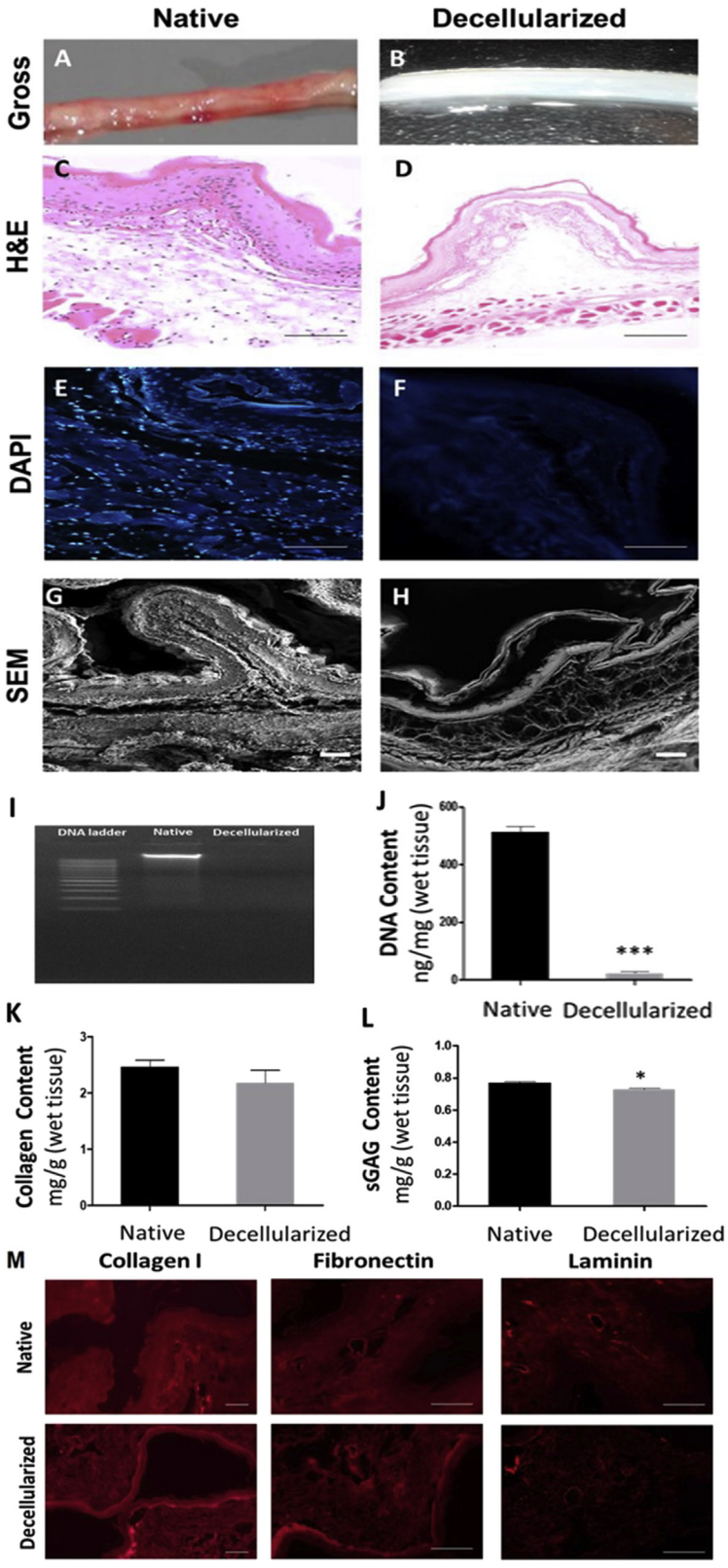

FIG. 1. Characterization of decellularized esophageal scaffolds. (A, B) Appearances of rat esophagi before and after decellularization; decellularized esophagi were transparent. (C, D) H&E staining showing the complete removal of cells and maintenance of the native structure in decellularized tissues, scale bar: 100 μm. (E, F) DAPI (4,6-diamidino-2-phenylindole) staining confirming cell-removal after decellularization, scale bar: 100 μm. (G, H) SEM images confirming the preservation of ECM structure in decellularized tissues), scale bar: 100 μm. (I) Agarose gel electrophoresis of the extracted DNA showing the absence of DNA in the decellularized group. (J) Graph showing significant decrease in amount of DNA after decellularization (***$P = 0.0004$). (K, L) Graphs showing non-significant (ns) decrease in collagen ($P = 0.0757$), and significant decrease in sulfated glycosaminoglycan (sGAG) (*$P = 0.0377$) after decellularization. (M) Immunofluorescent staining of collagen I, fibronectin, and laminin in the decellularized tissue compared to the native tissue, scale bar: 50 μm.

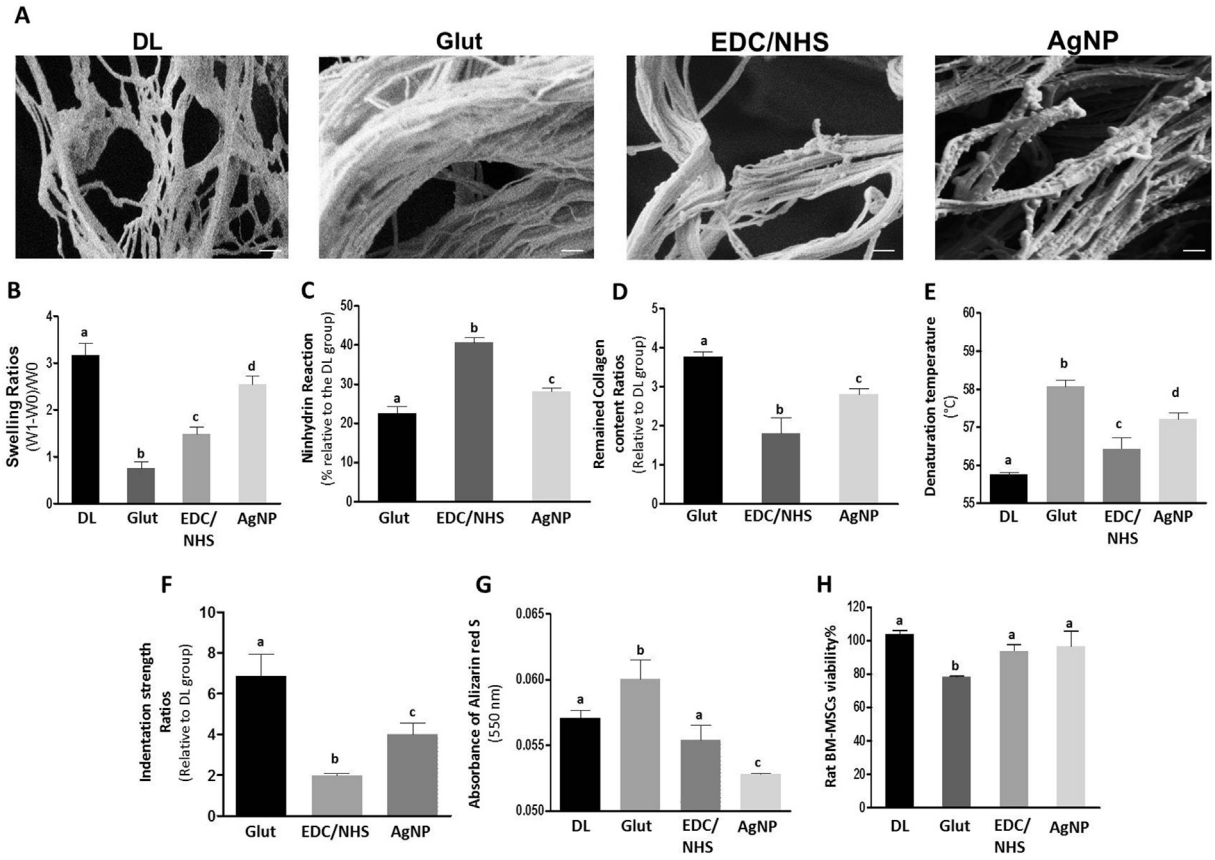

FIG. 2. The different beneficial effects and cytocompatibility of different decellularized esophageal scaffold modification. (A) Representative SEM images showing structural improvements in the sub-mucosal layer of the different modified esophagi in comparison with the decellularized esophagi, scale bar: 200 nm. (B) Graph showing swelling ratios [wet weight increase (W1-W0) to the initial dry weight (W0)] of decellularized and modified scaffold groups. The AgNP group revealed a higher swelling ratio compared with both the Glut and EDC/NHS groups. (C, D) Graphs showing the evaluation of *in vitro* collagenase-mediated biodegradation by quantifying ninhydrin reaction percentages, and ratios of insoluble collagen content for the different modified groups with respect to the decellularized group. (E) Graph showing the evaluation of thermal degradation based on the denaturation temperatures of samples from different groups. (F) Graph showing the ratios of indentation strengths of the samples from different groups. (G) Graph showing the absorbance of samples from each group following alizarin red S staining; these absorbance values determine the *in vitro* anti-calcification properties. (H) Graph showing cell viability percentage of rat BM-MSCs using an indirect MTT (3-[4,5-dimethyl (thiazol-2-yl)-3,5-diphenyl] tetrazolium bromide) assay. The mean ± SD values in the same graph that are indicated with different small letters (a, b, c, d) are significantly different from each other ($P < 0.05$).

bind to the hydrophobic areas in the scaffolds and/or form hydrogen bonds. Moreover, the nanoparticles were immobilized using the coupling reagent EDC/NHS, which improves the physical binding of AgNPs to the loaded scaffolds via the formation of stable amide bonds between the amine and the carboxyl functional groups of the scaffolds (12,14,19).

Decellularization protocol efficacy Results from our decellularization process demonstrated that complete decellularization was achieved without massive damage to the native-mimic structure of the decellularized tissues. Similar good decellularization efficacy for the esophagus was reported using different protocols in previous studies (4,31).

Ultra-structural morphology of the modified esophageal scaffolds After modifying the decellularized esophagi with glutaraldehyde, EDC/NHS, or AgNPs, results of SEM imaging of the different esophagi showed structural improvements of collagen fibers within the submucosal layer. Moreover, samples from the AgNP group displayed more regular coiled collagen fibers compared to the EDC/NHS group, and without the negative effects on pore spaces, like the case in the Glut group. This may be due to the unique properties of nanoparticles and their very large surface areas, which allow them to increase the coiling of collagen fibers without adversely affecting the porosity of the connected fibers (18,32,33).

Swelling test results for the modified esophageal scaffolds Results of the swelling test, which reflect porosities of the different modified esophageal scaffolds (34), showed that while all modifications decreased the swelling ratios, the AgNP group showed the highest swelling ratio, and the Glut group, the lowest. The high ability of water uptake seen in case of samples from the AgNP group may be due to the ability of AgNPs to bind with water via electrostatic interactions in watery environments and/or increase the scaffold surface network area, which in turn, increases the hydrophilic properties of the scaffold (35,36). In addition, the treatment of the AgNP-loaded scaffolds with EDC/NHS was performed for a short time for the immobilization of the nanoparticles. Therefore, this treatment method did not affect the porosity of the esophagus scaffolds in the AgNP group.

Structural properties of the modified esophageal scaffolds In the current study, the samples in the Glut group were the best in terms of increased resistance to *in vitro* enzymatic biodegradation, thermal degradation, and indentation following by those in the AgNP group; the differences between the two groups were significant. This is may be due to the fact that the *in vitro* collagenase biodegradation assay may depend mainly on collagen stability, and glutaraldehyde induced the crosslinking of collagen more than that of other ECM components such as elastin and glycoproteins, due to the abundant presence of free amine groups in

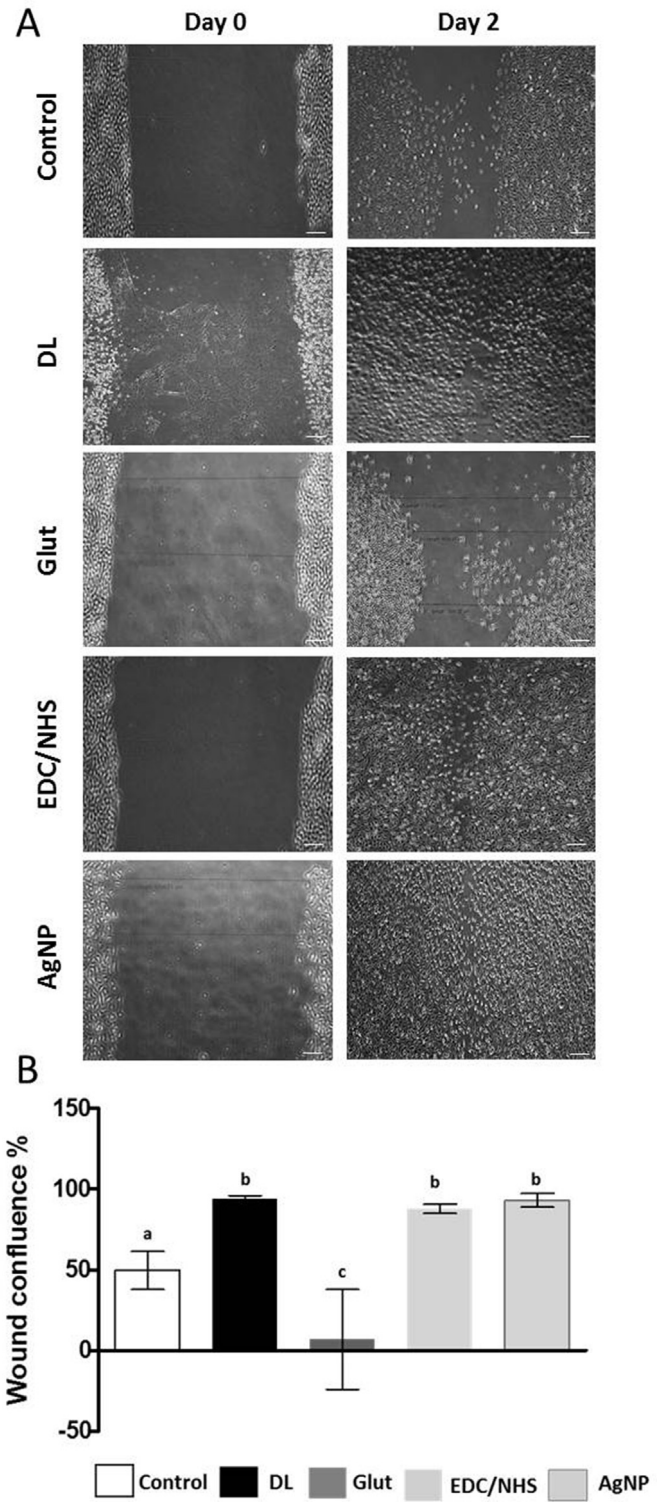

FIG. 3. The angiogenic properties of the different modified esophageal scaffolds. (A) Representative phase contrast images of the scratch wound assay showing the migration of EA.hy926 endothelial cells over the scraped areas in the different groups, scale bar: 200 μm. (B) Graph showing the quantitative analysis of the scratch wound assay by calculating the wound confluence percentages. Mean ± SD values in the same graph that are indicated with different small letters (a, b, c) are significantly different from each other ($P < 0.05$).

collagen and the lack of such groups in elastin and other proteins (6). In addition to the fact that enzyme biodegradation is more vigorous *in vitro* than in the *in vivo* environment, the *in vivo* condition is dependent on many other factors, mainly including the intensity of the host immune response, which alters the biodegradation process due to the effect of the collagenase secreted by inflammatory cells (18,37). With regards to this aspect, the fact that the highest values of thermal stability and indentation strength were observed in samples from the Glut group may be due to the effects of the hardness and low water contents of the Glut-modified scaffolds; these factors may have contributed towards increasing the mean values of these parameters.

The hardness and hydrophobic properties of the Glut-modified scaffolds are undesirable properties, as they may limit the chance of their successful transplantation (38–40). In any case, we can say that a considerable increase in the structural stability of the decellularized esophageal scaffolds and their resistance to degradation could be achieved using AgNPs (13,18,41–43). These results differ slightly from our results in porcine livers (18). In this previous study, the AgNPs increased the structural stability of porcine liver materials, but demonstrated an ability similar to that of glutaraldehyde with regards to increasing the resistance of the materials to collagenase degradation. This finding may be explained by the structural differences between the two organs.

***In vitro* anti-calcification properties of the modified esophageal scaffolds** With regards to the results of the analysis of *in vitro* anti-calcification properties, the scaffolds from the AgNP group showed the best resistance against mineral deposition and calcification; the *in vitro* calcification resistance of samples from the other groups was lower. This may be due to the high hydrophilicity of the AgNP-modified scaffolds, which decreases the tendency of mineral deposition, and the unspecific stability of the different ECM components including elastin during the incubation period. On the contrary, the high calcification tendency of the samples in the Glut group may be due to several reasons: (i) their hydrophobic properties may lead to the trapping of more minerals, (ii) presence of free aldehydes may lead to calcium binding, and (iii) lack of elastin stability. On the other hand, the suggested cause of calcification in the scaffolds from the DL and EDC/NHS groups is their weak structure, which spontaneously affects the elastin integrity, thereby enhancing the calcification (26,27,44,45).

Cytocompatibility of the modified esophageal scaffolds As the one of the most important characteristics of any modifying agent is that it be non-cytotoxic, cytocompatibility of the different modified esophagi was evaluated by means of an extraction-MTT assay using rat BM-MSCs, as this cell type is one that could be used for recellularization of the esophageal scaffolds. The results showed that the cellular viability was significantly decreased in the Glut group, while both EDC/NHS and AgNP groups did not display any toxic effects on cellular viability. This finding testified to the good cytocompatibility afforded by large AgNPs at a concentration of 5 μg/mL on modified esophageal scaffolds, and is in agreement with previous studies that investigated the cytocompatibility of AgNPs of similar size and concentration in human-derived stem cells (46,47).

Angiogenic properties of the modified esophageal scaffolds Samples from all groups in the study, except the Glut group, supported the *in vitro* migration and proliferation of endothelial cells in the *in vitro* scratch model. This may be because of the inhibitory effects of the aldehydes released from the glutaraldehyde-modified scaffolds (48); however, with regards to angiogenic properties, AgNPs have dual effects depending on their size and concentration. AgNPs with a size of 100 nm and at a concentration of 5 μg/ml have no cytotoxic effects on endothelial cells (18,49).

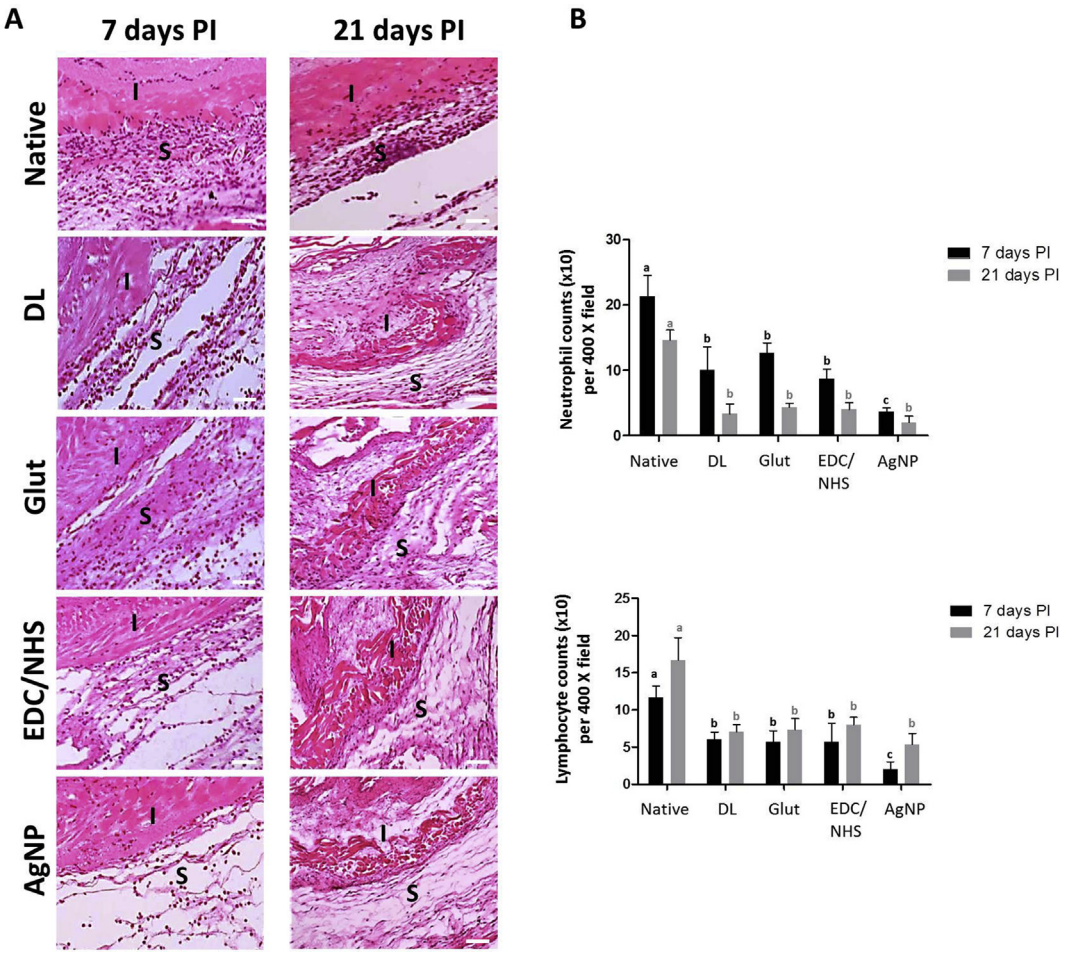

FIG. 4. Host immune reactions against scaffolds of the different groups: (A) Representative H&E staining images showing the inflammatory reactions surrounding implanted scaffolds (I and S, implanted and surrounding tissues, respectively) from different groups at 7 and 21 days post implantation (PI). The native group exhibited an intense host immune response, while the other groups showed only mild host responses, scale bar: 100 μm. (B) Graphs showing the mean ± SD values of different inflammatory cells at 7 and 21 days PI that were counted for five histological fields (400X) in the areas surrounding scaffolds in different groups. Different black and grey letters (a, b, c) indicate significant differences ($P < 0.05$) between the different groups at 7 and 21 days PI, respectively.

***In vivo* subcutaneous implantation of the modified esophageal scaffolds** We did not comprehensively examine the biodegradation of different implanted scaffolds, because (i) with the exception of the native and DL groups, significant *in vivo* changes in modified implanted tissues are difficult to find, unlike the case for the *in vitro* aggressive digestion process, and (ii) our focus was mainly on the host immune response that affects the regeneration process of the recellularized transplantable materials (37). In the microscopic examination of the different modified implanted scaffolds, the samples from the AgNP group showed the most promising results in terms of biocompatibility. Although the samples from all groups, except the native samples, showed reduced immune host responses, those in the AgNP group showed the lowest number of inflammatory cells at 7 and 21 days PI, compared to the other modified scaffold groups, with significant differences only at 7 days PI. This finding revealed that the biocompatibility of the scaffolds in the AgNP group may be improved due to the ability of the AgNPs to suppress the production of inflammatory cytokines such as the different pro-inflammatory interleukins, tumor necrosis factor, and interferon gamma, and scavenge free radicals (50–52). Subsequently, the host immune response decreased, and the immunogenicity of the AgNP-loaded esophageal scaffolds was suppressed. Therefore, the durability of the transplanted esophageal scaffold could potentially be increased in the low inflammatory environment, allowing the scaffolds to maintain their integrity until the recellularized cells build their own new scaffold materials.

With regards to the macrophage phenotype, which gives an impression about the acceptance or rejection of the transplanted implants, the M1/M2 ratios of the samples in the Glut group were altered compared to those of all the unmodified and modified decellularized groups; the samples from the Glut group showed mixed M1/M2 responses, especially at the early stage of implantation. This is maybe due to the cytotoxic effects of glutaraldehyde, which may lead to the increase of the proinflammatory cytokine levels, thereby causing an increase in the number of M1 macrophages (53). Such an alteration was not observed in case of samples from the other modified groups, which showed higher M2 expression, indicating better biocompatibility (54).

Taking the above findings into account, our study concluded that the conjugation of AgNPs into decellularized esophageal scaffolds improves the morphology of their collagen fibers, allows for good porosity, increases their resistance to degradation, indentation, and calcification, and improves their *in vivo* biocompatibility. This novel method of tissue modification has the potential to open new doors in the generation of highly-biocompatible esophageal scaffolds for esophageal tissue engineering.

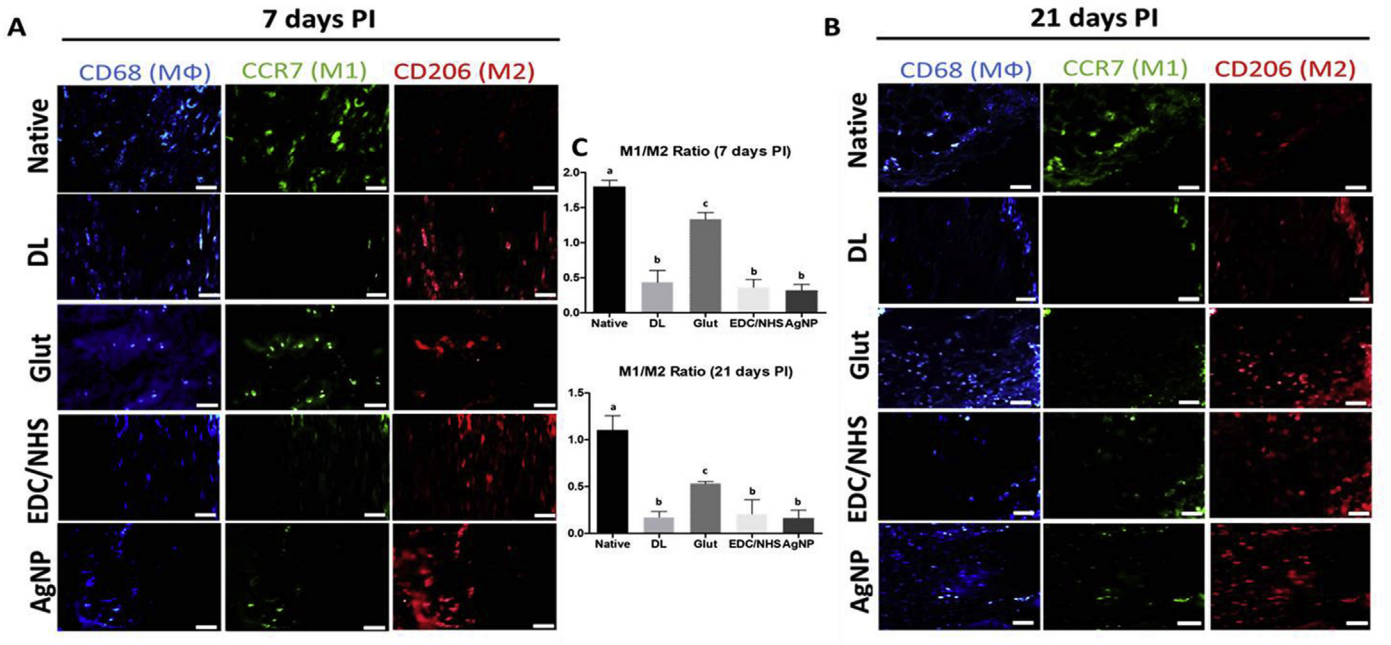

FIG. 5. Polarization of macrophages in the different groups: (A, B) Representative immunofluorescent images showing the polarization of macrophages in the different groups at 7 and 21 days post implantation (PI), scale bar: 50 μm. (C) Graphs showing means ± SD values of M1/M2 ratios in the different groups at 7 and 21 days PI. The Glut group showed the highest ratios among the unmodified decellularized and modified groups and the differences were significant. No significant differences among DL, EDC/NHS and AgNP groups were found. Mean ± SD values with different letters (a, b, c) are significantly different from each other ($P < 0.05$).

ACKNOWLEDGMENTS

This work was supported by the Cooperative Research Program for Agriculture Science & Technology Development (Project No. PJ01100201), Rural Development Administration, Republic of Korea.

The authors certify to have no conflict of interest.

Tarek Saleh and Ebtehal Ahmed designed and performed the research experiments, data analysis/interpretation and wrote the manuscript; Yu-Lina, Ho-Hyun Kwak, Byung-Jae Kang, Kyung-Mee Park, Ki-Young Choi, and Byeong-Moo Kim contributed to data discussion. Kang K-S involved in financial support, and final approval of manuscript. Woo H-M participated in study design, interpretation of data, approval of the article and secured funding.

References

1. **Hussey, G. S., Cramer, M. C., and Badylak, S. F.:** Extracellular matrix bioscaffolds for building gastrointestinal tissue, Cell. Mol. Gastroenterol. Hepatol., **5**, 1–13 (2018).
2. **Hussey, G. S., Keane, T. J., and Badylak, S. F.:** The extracellular matrix of the gastrointestinal tract: a regenerative medicine platform, Nat. Rev. Gastroenterol. Hepatol., **14**, 540–552 (2017).
3. **Londono, R. and Badylak, S. F.:** Regenerative medicine strategies for esophageal repair, Tissue Eng. Part B Rev., **21**, 393–410 (2015).
4. **Bhrany, A. D., Lien, C. J., Beckstead, B. L., Futran, N. D., Muni, N. H., Giachelli, C. M., and Ratner, B. D.:** Crosslinking of an oesophagus acellular matrix tissue scaffold, Tissue Eng. Regen. Med., **2**, 365–372 (2008).
5. **Koch, H., Graneist, C., Emmrich, F., Till, H., Metzger, R., Aupperle, H., Schierle, K., Sack, U., and Boldt, A.:** Xenogenic esophagus scaffolds fixed with several agents: comparative *in vivo* study of rejection and inflammation, BioMed Res. Int., **2012**, 948320 (2012).
6. **Tam, H., Zhang, W., Infante, D., Parchment, N., Sacks, M., and Vyavahare, N.:** Fixation of bovine pericardium-based tissue biomaterial with irreversible chemistry improves biochemical and biomechanical properties, J. Cardiovasc. Transl. Res., **10**, 194–205 (2017).
7. **Hussein, K. H., Park, K.-M., Lee, Y.-S., Woo, J.-S., Kang, B.-J., Choi, K.-Y., Kang, K.-S., and Woo, H.-M.:** New insights into the pros and cons of crosslinking decellularized bioartificial organs, Int. J. Artif. Organs, **40**, 136–141 (2017).
8. **Ma, B., Wang, X., Wu, C., and Chang, J.:** Crosslinking strategies for preparation of extracellular matrix-derived cardiovascular scaffolds, Regen. Biomater., **1**, 81–89 (2014).
9. **Ostdiek, A. M., Ivey, J. R., Grant, D. A., Gopaldas, J., and Grant, S. A.:** An in vivo study of a gold nanocomposite biomaterial for vascular repair, Biomaterials, **65**, 175–183 (2015).
10. **Grant, S. A., Smith, S. E., Schmidt, H., Pfeiffer, F., Kuroki, K., Sherman, S., White, R., and Grant, D. A.:** In vivo bone tunnel evaluation of nanoparticle-grafts using an ACL reconstruction rabbit model, J. Biomed. Mater. Res. A, **105**, 1071–1082 (2017).
11. **Nair, R. S., Ameer, J. M., Alison, M. R., and Anilkumar, T. V.:** A gold nanoparticle coated porcine cholecyst-derived bioscaffold for cardiac tissue engineering, Colloids Surf. B Biointerfaces, **157**, 130–137 (2017).
12. **Saleh, T. M., Ahmed, E. A., Yu, L., Kwak, H.-H., Hussein, K. H., Park, K.-M., Kang, B.-J., Choi, K.-Y., Kang, K.-S., and Woo, H.-M.:** Incorporation of nanoparticles into transplantable decellularized matrices: applications and challenges, Int. J. Artif. Organs, **41**, 421–430 (2018).
13. **Kwan, K. H., Liu, X., To, M. K., Yeung, K. W., Ho, C.-m., and Wong, K. K.:** Modulation of collagen alignment by silver nanoparticles results in better mechanical properties in wound healing, Nanomedicine, **7**, 497–504 (2011).
14. **Ravindran, A., Chandran, P., and Khan, S. S.:** Biofunctionalized silver nanoparticles: advances and prospects, Colloids Surf. B Biointerfaces, **105**, 342–352 (2013).
15. **Beck, I., Hotowy, A., Sawosz, E., Grodzik, M., Wierzbicki, M., Kutwin, M., Jaworski, S., and Chwalibog, A.:** Effect of silver nanoparticles and hydroxyproline, administered in ovo, on the development of blood vessels and cartilage collagen structure in chicken embryos, Arch. Anim. Nutr., **69**, 57–68 (2015).
16. **Song, J., Zhang, P., Cheng, L., Liao, Y., Xu, B., Bao, R., Wang, W., and Liu, W.:** Nano-silver in situ hybridized collagen scaffolds for regeneration of infected full-thickness burn skin, J. Mater. Chem. B, **3**, 4231–4241 (2015).
17. **Murphy, M., Ting, K., Zhang, X., Soo, C., and Zheng, Z.:** Current development of silver nanoparticle preparation, investigation, and application in the field of medicine, J. Nanomater., **2015**, 696918 (2015).
18. **Saleh, T., Ahmed, E., Yu, L., Hussein, K., Park, K.-M., Lee, Y.-S., Kang, B.-J., Choi, K.-Y., Choi, S., and Kang, K.-S.:** Silver nanoparticles improve structural stability and biocompatibility of decellularized porcine liver, Artif. Cells Nanomed. Biotechnol., **46**, 273–284 (2018).
19. **Gu, L., Shan, T., Ma, Y.-X., Tay, F. R., and Niu, L.:** Novel biomedical applications of crosslinked collagen, Trends Biotechnol., **37**, 464–491 (2019).
20. **Yan, L. P., Wang, Y. J., Ren, L., Wu, G., Caridade, S. G., Fan, J. B., Wang, L. Y., Ji, P. H., Oliveira, J. M., and Oliveira, J. T.:** Genipin-cross-linked collagen/chitosan biomimetic scaffolds for articular cartilage tissue engineering applications, J. Biomed. Mater. Res. A, **95**, 465–475 (2010).

21. **Poursamar, S. A., Hatami, J., Lehner, A. N., da Silva, C. L., Ferreira, F. C., and Antunes, A. P. M.:** Gelatin porous scaffolds fabricated using a modified gas foaming technique: characterisation and cytotoxicity assessment, Mater. Sci. Eng. C Mater. Biol. Appl., **48**, 63–70 (2015).
22. **Ragaert, K., De Somer, F., Somers, P., De Baere, I., Cardon, L., and Degrieck, J.:** Flexural mechanical properties of porcine aortic heart valve leaflets, J. Mech. Behav. Biomed. Mater., **13**, 78–84 (2012).
23. **Cheung, H. K., Han, T. T. Y., Marecak, D. M., Watkins, J. F., Amsden, B. G., and Flynn, L. E.:** Composite hydrogel scaffolds incorporating decellularized adipose tissue for soft tissue engineering with adipose-derived stem cells, Biomaterials, **35**, 1914–1923 (2014).
24. **Tse, J. R. and Long, J. L.:** Microstructure characterization of a decellularized vocal fold scaffold for laryngeal tissue engineering, Laryngoscope, **124**, 326–331 (2014).
25. **Rodriguez, I. A., Sell, S. A., McCool, J. M., Saxena, G., Spence, A. J., and Bowlin, G. L.:** A preliminary evaluation of lyophilized gelatin sponges, enhanced with platelet-rich plasma, hydroxyapatite and chitin whiskers for bone regeneration, Cells, **2**, 244–265 (2013).
26. **Zhai, W., Zhang, H., Wu, C., Zhang, J., Sun, X., Zhang, H., Zhu, Z., and Chang, J.:** Crosslinking of saphenous vein ECM by procyanidins for small diameter blood vessel replacement, J. Biomed. Mater. Res. B Appl. Biomater., **102**, 1190–1198 (2014).
27. **Mendoza-Novelo, B., Alvarado-Castro, D. I., Mata-Mata, J. L., Cauich-Rodríguez, J. V., Vega-González, A., Jorge-Herrero, E., Rojo, F. J., and Guinea, G. V.:** Stability and mechanical evaluation of bovine pericardium cross-linked with polyurethane prepolymer in aqueous medium, Mat. Sci. Eng. C Mater., **33**, 2392–2398 (2013).
28. **Zhang, L. and Chan, C.:** Isolation and enrichment of rat mesenchymal stem cells (MSCs) and separation of single-colony derived MSCs, J. Vis. Exp., **37**, e1852 (2010).
29. **Goodwin, A. M.:** In vitro assays of angiogenesis for assessment of angiogenic and anti-angiogenic agents, Microvasc. Res., **74**, 172–183 (2007).
30. **Sanskriti, I. and Upadhyay, K.:** Cysteine, homocysteine and glutathione guided hierarchical self-assemblies of spherical silver nanoparticles paving the way for their naked eye discrimination in human serum, New J. Chem., **41**, 4316–4321 (2017).
31. **Ozeki, M., Narita, Y., Kagami, H., Ohmiya, N., Itoh, A., Hirooka, Y., Niwa, Y., Ueda, M., and Goto, H.:** Evaluation of decellularized esophagus as a scaffold for cultured esophageal epithelial cells, J. Biomed. Mater. Res. A, **79**, 771–778 (2006).
32. **Rath, G., Hussain, T., Chauhan, G., Garg, T., and Goyal, A. K.:** Collagen nanofiber containing silver nanoparticles for improved wound-healing applications, J. Drug Target., **24**, 520–529 (2016).
33. **Alarcon, E. I., Udekwu, K. I., Noel, C. W., Gagnon, L. B.-P., Taylor, P. K., Vulesevic, B., Simpson, M. J., Gkotzis, S., Islam, M. M., and Lee, C.-J.:** Safety and efficacy of composite collagen–silver nanoparticle hydrogels as tissue engineering scaffolds, Nanoscale, **7**, 18789–18798 (2015).
34. **Mattei, G., Di Patria, V., Tirella, A., Alaimo, A., Elia, G., Corti, A., Paolicchi, A., and Ahluwalia, A.:** Mechanostructure and composition of highly reproducible decellularized liver matrices, Acta Biomater., **10**, 875–882 (2014).
35. **Ahmed, E. M. and Aggor, F. S.:** Swelling kinetic study and characterization of crosslinked hydrogels containing silver nanoparticles, J. Appl. Polym. Sci., **117**, 2168–2174 (2010).
36. **Liu, B. S. and Huang, T. B.:** Nanocomposites of genipin-crosslinked chitosan/silver nanoparticles-structural reinforcement and antimicrobial properties, Macromol. Biosci., **8**, 932–941 (2008).
37. **Wu, X., Wang, Y., Wu, Q., Li, Y., Li, L., Tang, J., Shi, Y., Bu, H., Bao, J., and Xie, M.:** Genipin-crosslinked, immunogen-reduced decellularized porcine liver scaffold for bioengineered hepatic tissue, J. Tissue Eng. Regen. Med., **12**, 417–426 (2015).
38. **Meuris, B., Verbeken, E., and Flameng, W.:** Prevention of porcine aortic wall calcification by acellularization: necessity for a non-glutaraldehyde-based fixation treatment, J. Heart Valve Dis., **14**, 358–363 (2005).
39. **Oryan, A., Kamali, A., Moshiri, A., Baharvand, H., and Daemi, H.:** Chemical crosslinking of biopolymeric scaffolds: current knowledge and future directions of crosslinked engineered bone scaffolds, Int. J. Biol. Macromol., **107**, 678–688 (2018).
40. **Guo, S., Wang, Q., Sun, J., Liao, X., and Wang, Z.-s.:** Study on the influence of moisture content on thermal stability of propellant, J. Hazard. Mater., **168**, 536–541 (2009).
41. **Srivatsan, K. V., Duraipandy, N., Begum, S., Lakra, R., Ramamurthy, U., Korrapati, P. S., and Kiran, M. S.:** Effect of curcumin caged silver nanoparticle on collagen stabilization for biomedical applications, Int. J. Biol. Macromol., **75**, 306–315 (2015).
42. **Socrates, R., Sakthivel, N., Rajaram, A., Ramamoorthy, U., and Kalkura, S. N.:** Novel fibrillar collagen–hydroxyapatite matrices loaded with silver nanoparticles for orthopedic application, Mater. Lett., **161**, 759–762 (2015).
43. **Wang, C., Li, J., Sun, S., Li, X., Wu, G., Wang, Y., Xie, F., and Huang, Y.:** Controlled growth of silver nanoparticles on carbon fibers for reinforcement of both tensile and interfacial strength, RSC Adv., **6**, 14016–14026 (2016).
44. **Narine, K., Somers, P., Bouchez, S., Van Nooten, G., Cox, E., Gasthuys, F., Cornelissen, M., and Sparks, L.:** Acellular porcine and kangaroo aortic valve scaffolds show more intense immune-mediated calcification than cross-linked Toronto SPV valves in the sheep model, Interact. Cardiovasc. Thorac. Surg., **5**, 544–549 (2006).
45. **Okoshi, T. and Noishiki, Y.:** Encyclopedic handbook of biomaterials and bioengineering: v. 1-2, applications, pp. 1153–1171, in: Wise, D. L. (Ed.), New frontiers of biomaterials for cardiovacular surgery. CRC Press (1995).
46. **Greulich, C., Kittler, S., Epple, M., Muhr, G., and Köller, M.:** Studies on the biocompatibility and the interaction of silver nanoparticles with human mesenchymal stem cells (hMSCs), Langenbeck's Arch. Surg., **394**, 495–502 (2009).
47. **Sengstock, C., Diendorf, J., Epple, M., Schildhauer, T. A., and Köller, M.:** Effect of silver nanoparticles on human mesenchymal stem cell differentiation, Beilstein J. Nanotechnol., **5**, 2058–2069 (2014).
48. **Eybl, E., Griesmacher, A., Grimm, M., and Wolner, E.:** Toxic effects of aldehydes released from fixed pericardium on bovine aortic endothelial cells, J. Biomed. Mater. Res., **23**, 1355–1365 (1989).
49. **Zhang, X.-F., Shen, W., and Gurunathan, S.:** Silver nanoparticle-mediated cellular responses in various cell lines: an in vitro model, Int. J. Mol. Sci., **17**, 1603 (2016).
50. **Hebeish, A., El-Rafie, M., El-Sheikh, M., Seleem, A. A., and El-Naggar, M. E.:** Antimicrobial wound dressing and anti-inflammatory efficacy of silver nanoparticles, Int. J. Biol. Macromol., **65**, 509–515 (2014).
51. **You, C., Li, Q., Wang, X., Wu, P., Ho, J. K., Jin, R., Zhang, L., Shao, H., and Han, C.:** Silver nanoparticle loaded collagen/chitosan scaffolds promote wound healing via regulating fibroblast migration and macrophage activation, Sci. Rep., **7**, 10489 (2017).
52. **Manikandan, R., Manikandan, B., Raman, T., Arunagirinathan, K., Prabhu, N. M., Jothi Basu, M., Perumal, M., Palanisamy, S., and Munusamy, A.:** Biosynthesis of silver nanoparticles using ethanolic petals extract of *Rosa indica* and characterization of its antibacterial, anticancer and anti-inflammatory activities, Spectrochim. Acta Mol. Biomol. Spectrosc., **138**, 120–129 (2015).
53. **Gao, M., Wang, Y., He, Y., Li, Y., Wu, Q., Yang, G., Zhou, Y., Wu, D., Bao, J., and Bu, H.:** Comparative evaluation of decellularized porcine liver matrices cross-linked with different chemical and natural crosslinking agents, Xenotransplantation, **26**, e12470 (2019).
54. **Spiller, K. L., Anfang, R. R., Spiller, K. J., Ng, J., Nakazawa, K. R., Daulton, J. W., and Vunjak-Novakovic, G.:** The role of macrophage phenotype in vascularization of tissue engineering scaffolds, Biomaterials, **35**, 4477–4488 (2014).